Baltic Astronomy, vol. 21, 523–529, 2012

KINEMATIC MODELING OF DISTANT GALAXIES

Rain Kipper[1,2], Elmo Tempel[2,3] and Antti Tamm[2]

[1] *Institute of Physics, University of Tartu, 51010 Tartu, Estonia; rain@aai.ee*

[2] *Tartu Observatory, 61602 Tõravere, Estonia*

[3] *National Institute of Chemical Physics and Biophysics, Tallinn, Estonia*

Received: 2012 August 9; accepted: 2012 September 14

Abstract. Evolution of galaxies is one of the most actual topics in astrophysics. Among the most important factors determining the evolution are two galactic components which are difficult or even impossible to detect optically: the gaseous disks and the dark matter halo. We use deep Hubble Space Telescope images to construct a two-component (bulge + disk) model for stellar matter distribution of galaxies. Properties of the galactic components are derived using a three-dimensional galaxy modeling software, which also estimates disk thickness and inclination angle. We add a gas disk and a dark matter halo and use hydrodynamical equations to calculate gas rotation and dispersion profiles in the resultant gravitational potential. We compare the kinematic profiles with the Team Keck Redshift Survey observations. In this pilot study, two galaxies are analyzed deriving parameters for their stellar components; both galaxies are found to be disk-dominated. Using the kinematical model, the gas mass and stellar mass ratio in the disk are estimated.

Key words: galaxies: kinematics and dynamics – galaxies: structure

1. INTRODUCTION

Understanding the evolution of galactic structures is of uttermost importance in astrophysics. The knowledge of the processes determining the morphology, star formation history and intrinsic kinematics of galaxies give us the clues about the general cosmological framework: fundamental cosmological parameters, properties of dark matter, cosmic recycling and enrichment of baryonic matter, etc. However, several key aspects of galaxy evolution are poorly understood so far.

Owing to extensive surveys, like the Sloan Digital Sky Survey (York et al. 2000), the general structure of galaxies is quite well established (e.g., Simard et al. 2011; Lackner & Gunn 2012). For a direct tracing of evolutionary effects, the local galaxy sample has to be compared to galaxies at cosmologically significant distances. Unfortunately, only small samples of distant galaxies have been studied so far. From photometric decomposition of galaxies out to redshift $z \simeq 6$ (e.g., Tamm & Tenjes 2006; Fathi et al. 2012), it has been shown that sizes of galaxy disks decrease with the redshift, in general accordance with simulations.

On the other hand, studies of the evolution of the intrinsic kinematics (and thus the gravitation potential and dynamical formation history) of galaxies do not extend much beyond $z \simeq 1$. It has been shown that the evolution of the Tully-Fisher relation is mild or missing over this period (Fernández Lorenzo et al. 2010; Miller et al. 2011).

In more detailed studies the photometric and kinematic data are used self-consistently to split the structure of galaxies into contributions by individual stellar, gaseous and dark matter components (Tenjes et al. 1994, 1998; Tempel & Tenjes 2006; Chemin et al . 2011; Jardel et al. 2011). However, for higher redshift objects the observational data rarely provide possibilities for such analyses (Tamm & Tenjes 2003, 2005).

In the present study we have used both photometric and kinematic observations to study the structure of distant disk-dominated galaxies. We have applied a simple bulge + disk model on deep Hubble Space Telescope observations. Using the data for gas kinematics, a gas disk component was added to the model. Masses of the components were derived by solving the isotropic Jeans equations.

Throughout this paper we assume the Friedmann-Robertson-Walker cosmological model with the total matter density $\Omega_{\rm m} = 0.27$, dark energy density $\Omega_\Lambda = 0.73$, and the Hubble constant $H_0 = 71\,{\rm km\,s^{-1}Mpc^{-1}}$.

2. THE DATA

Photometry of galaxies is based on the deep Hubble Space Telescope ACS camera observations in the GOODS project (Giavalisco et al. 2004). Modeling is based on z filter observations, in which young stars and dust have the smallest effect. Initial data reduction, including dithering (Mutchler & Cox 2001) to $0.03''$/pixel had been done by the GOODS team. Intensity counts were transformed into magnitudes using the formula

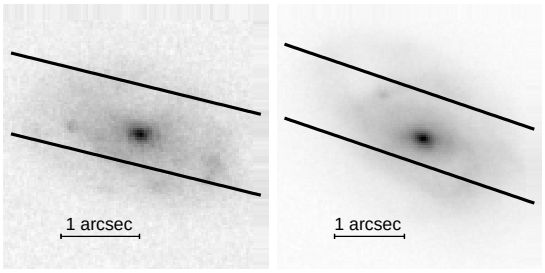

Fig. 1. Photometric images of two galaxies (left TKRS 2568, right TKRS 9059) in the z filter, with the positions of the spectrograph slit overplotted.

$$m = -2.5\log_{10}(N) + ZP, \tag{1}$$

where N are the electron counts per second in CCD pixel and ZP is the zero point of the used filter. According to Sirianni et al. (2005), the zero point for the z filter is 24.86 mag. We took 4.51 mag as the value of solar luminosity.

Figure 1 shows the z filter images of the studied galaxies, with the spectrograph slit positions and sizes indicated. Both galaxies have been selected to be disk-dominated objects with relatively good spectroscopic observations.

We used spectroscopic observations from the Team Keck Redshift Survey (TKRS; Wirth et al. 2004) of galaxies in the GOODS field using the DEIMOS spectrograph of the Keck II telescope. They have measured the [O II] 3727 Å emission line along the slit roughly parallel to the major axes of galaxies. The slit width was $1''$, which is comparable with the galaxy size. During spectroscopic observations

the seeing was 0.6″to 1″.

The original sample contains the rotation curves and velocity dispersion profiles of 380 galaxies extracted by Weiner et al. (2006) from the TKRS survey data. Since edge-on galaxies are difficult to use for photometric analysis and the face-on ones for kinematic analysis, we chose galaxies with intermediate inclination angles. Additional selection was based on the symmetry, spatial and velocity extent of the observed kinematics, required for reliable modeling. Approximately 10% of the galaxies matched these criteria. In this study we present the analysis of two galaxies (TKRS 2568 and TKRS 9059) which have good rotation and dispersion profiles and have also regular and disk-dominated morphology. The nomenclature is the same as used by Weiner et al. (2006).

3. THE MODEL

We used a three-dimensional model to describe the structure of each galaxy, briefly reviewed below. Details of the general model are given in Tempel et al. (2010, 2011).

3.1. Photometric model

The model galaxy is received as a superposition of its individual stellar components. In the present study we used a two-component model: bulge + disk. The light distribution of both components are approximated by the Einasto law,

$$l(a) = l(0) \exp\left[-\left(a/ka_0\right)^{1/N}\right], \tag{2}$$

where $l(0) = hL/(4\pi q a_0^3)$ is the central density and L is the component luminosity; a_0 is the mean harmonic radius and $a = \sqrt{R^2 + z^2/q}$, where R and z are cylindrical coordinates and q is the axial ratio of a component. The coefficients h and k are normalizing parameters, dependent on N.

These components are projected onto the sky plane using the following equation:

$$L(X,Y) = 2\sum_j \frac{q_j}{Q_j} \int_A^\infty \frac{l_j(a)a\,da}{\sqrt{a^2 - A^2}}, \tag{3}$$

where $Q^2 = \cos^2 i + q^2 \sin^2 i$ is the apparent axial ratio, i is the inclination angle of a galaxy, $A = \sqrt{X^2 + Y^2/Q^2}$ is the major semi-axis of the equidensity ellipse of the projected light distribution. The summation is made over galaxy components.

We estimated the correctness of the model fit, using the χ^2 value, defined by the sum of the squared differences of the model and observational pictures.

For minimizing χ^2 we gave a physically justified initial guess for the parameters ourselves. In the next step, the parameter values were specified using the downhill simplex method of Nelder and Mead from the Numerical Recipe library.

The photometric model gave us the stellar component (bulge and disk) parameters (a_0, q, N, L) and the inclination angle of a galaxy. These parameters were kept fixed during the following dynamical modeling.

3.2. Dynamical model

The dynamical model is based on the density distributions of the stellar components (bulge and disk), the gas disk and the dark matter halo. Density profiles

of the stellar components have the same distribution as the luminous components; a constant mass-to-light ratio was assumed, different for bulge and disk. The gas disk and dark matter parameters are derived during dynamical modeling. For describing the gas disk density distribution, we used Eq. (2). For the dark matter distribution, we used the Einasto profile in another form, which is becoming increasingly popular for this purpose:

$$\rho_{\rm Einasto} = \rho_{\rm c} \exp\left\{-d_n\left[(r/r_{\rm c})^{1/n} - 1\right]\right\}, \tag{4}$$

where n is in principle a free parameter. According to N-body simulations, we take $n = 6.0$ (Merritt et al. 2006; Navarro et al. 2010). The term d_n is a function of n in a way that $\rho_{\rm c}$ is the density at $r_{\rm c}$ defining a half-mass radius. The value of d_n is 17.67 for $n = 6$ (Merritt et al. 2006).

Dynamics of a galaxy was calculated from the potential and density distributions using the Jeans equations. For simplicity, axisymmetry and stationarity of the galaxy were assumed for solving the Jeans equations. Since the observed dynamics is based on gas motions, we could use the isotropic Jeans equations. The Jeans equations were thus used in the form

$$\frac{\partial(\rho\sigma^2)}{\partial R} + \frac{\rho V_\varphi^2}{R} + \rho\frac{\partial\Phi}{\partial R} = 0, \quad \tfrac{\partial}{\partial z}\rho\sigma^2 + \rho\tfrac{\partial\Phi}{\partial z} = 0, \tag{5}$$

where Φ is the sum of potentials of galaxy components, V_φ is the rotational velocity, σ is the dispersion of velocities and ρ is the gas disk density distribution; R and z are cylindrical coordinates.

From these equations the rotational velocity and velocity dispersions were derived

$$V_\varphi^2(R,z) = \frac{-R}{\rho}\left(\frac{\partial(\int_z^\infty \rho\frac{\partial\Phi}{\partial z}{\rm d}z')}{\partial R} + \rho\frac{\partial\Phi}{\partial R}\right), \tag{6}$$

$$\sigma^2(R,z) = \rho^{-1}\int_z^\infty \rho(R,z')\frac{\partial\Phi(R,z')}{\partial z}\,dz'. \tag{7}$$

To make the modeled data comparable with observations, we needed to find the line-of-sight projected velocity distributions. For constructing the line-of-sight distribution we applied a Gaussian velocity profile (based on V_φ and σ) in every point along the line of sight, and integrated them using the square of gas density as a weight. The projected velocity profile $F_{(X,Y)}(V)$ corresponding to each line of sight (X, Y) was found using the equation

$$F_{(X,Y)}(V) = \int_X^\infty \frac{\sum_{j=1}^{2}\left[l_{\rm gas}(R,z_j)\, f_{(R,z)}(V)\right]}{\sin i\sqrt{R^2 - X^2}} R\,dR, \tag{8}$$

$$z_{1,2} = \frac{Y}{\sin i} \pm \frac{\sqrt{R^2 - X^2}}{\tan i}, \tag{9}$$

where $l_{\rm gas}(R,z)$ denotes the spatial gas density (given by Eq. (2)) and $f_{(R,z)}(V)$ is the corresponding line-of-sight Gaussian velocity profile at a given point (R,z) in the galaxy, calculated on the basis of Eqs. (6) and (7).

Table 1. Parameters of the galaxy models.

ID	z	i [deg]	Comp	a_0 [kpc]	q	N	$L_{\rm total}$ $[10^{10}L_\odot]$	M $[10^{10}M_\odot]$
2568	0.488	49	Bulge	0.9	1.0	5.1	2.4	7.0
			Stellar disk	6.68	0.2	0.5	22.3	7.0
			Gas disk	8.0	0.1	0.1		1.0
9059	0.253	65	Bulge	1.2	1.0	6.0	3.7	4.8
			Stellar disk	5.95	0.2	0.7	19.1	7.0
			Gas disk	10.0	0.1	0.2		3.0

3.3. Comparing the velocity profile with observations

The observational data points of velocity dispersion and rotation are given along the spectroscopic slit. To compare these data with our model, we had to take into account the width of the slit and seeing. To achieve this we firstly calculated the model output as a pixel map, where each pixel represents a line-of-sight integrated velocity distribution profile.

The atmospheric effects were taken into account by convolution of the velocity profile map with a Gaussian seeing function. During the observations the seeing changed from $0.6''$ to $1''$, therefore we used a Gaussian seeing kernel with a width of $0.8''$. Since the spectroscopic slit was of similar width ($1''$), the accuracy of the seeing kernel was not very important.

Trying to take into account the slit width, we summed the velocity profiles along the slit in bins, centered to the given observational points. We used the square of spatial density of gas as a weight for the summation. Thus the final model velocity profile allows a direct comparison to the observational points.

For fitting the model galaxy to the observed kinematics, we used the structure of the bulge and disk as derived during the photometric analysis. We used the maximal disk method, ascribing as much mass to the disk as allowed by the observed rotation curve. Subsequently, the masses of the bulge, gas disk and dark matter halo were derived to achieve the best fit to the observed kinematics.

4. RESULTS

Using the IRAF task *ellipse*, we found elliptically averaged one-dimensional profiles of the model and the observed images using the same ellipse parameters for both cases. Figure 2 shows the model and the observed profiles in the z filter, together with the contributions by the bulge and disk components. The modeled galaxy parameters are given in Table 1. The results of the dynamical modeling are presented in Figure 3, showing the observed kinematic profiles together with the modeled ones.

Due to degeneracy, the found parameters are one of the possible parameter sets that fit the galaxy. For this the parameters of the dark matter halo are responsible, because they originate from the inner parts of the galaxy, where the potential is dominated by the luminous components.

TKRS 2568 is a disk-dominated (bulge to total luminosity ratio $\mathrm{B/T} = 0.1$) galaxy at redshift $z = 0.488$. The inclination angle is 49°, which makes the galaxy suitable for kinematic and photometric analysis. It has clumpy disk structure, which could refer to a forming bulge (Conselice 2003). As can be seen from Figures 2 and 3, the four-component model (bulge + disk + gas + dark matter halo) gives

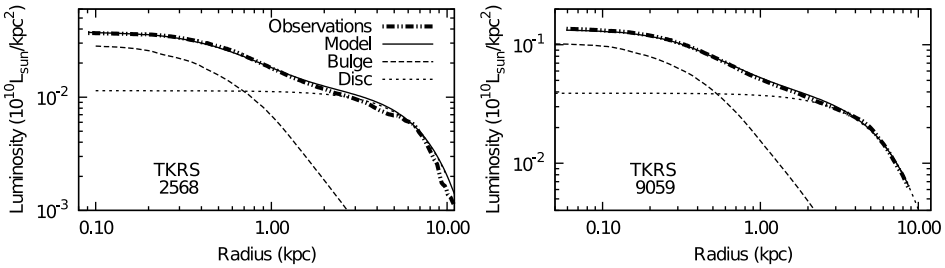

Fig. 2. Results of photometric modeling for the z filter.

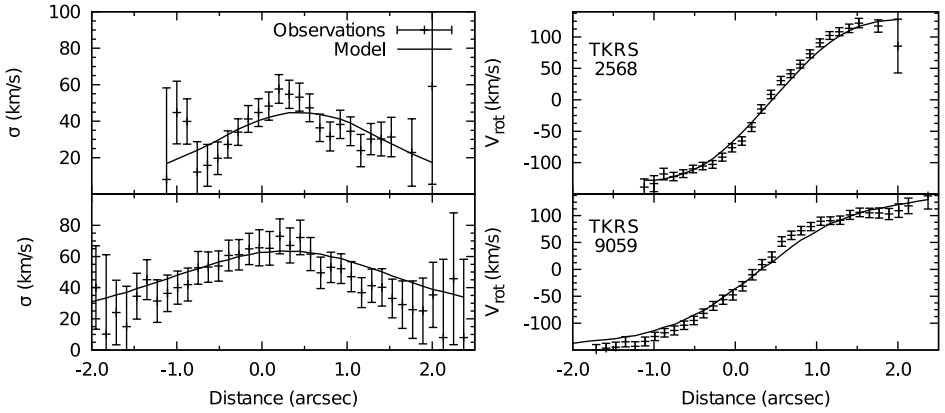

Fig. 3. Results of dynamical modeling for TKRS 2568 and TKRS 9059. The x axis is from the slit center.

a good fit to the photometric and kinematic observations. Since the observed rotation curve does not reach the expected plateau supported by the gravitational potential of dark matter halo, the parameters for the dark matter component are highly uncertain.

TKRS 9059 is also disk-dominated galaxy (B/T = 0.14) at redshift 0.253. In the outer regions of the galaxy stellar streams or tilted spiral arms, maybe be related to a recent merger or accretion event, are seen. They make the interpretation of the kinematic data less reliable: stationarity might not be fully achieved, which is also seen from higher dispersion errors. The inclination angle (67°) is determined from the inner, expected disk-dominated region. A good fit to the observed kinematics does not require the use of a dark matter halo component. Although not justified by the current cosmological paradigm, the data do not allow us to give any constraints to the possible dark matter halo.

In general, resulting from the model constraints and the limited depth of observations, the derived galactic components are somewhat degenerate and the presence of the dark matter halos remain not confirmed. However, the modeling software enables to brake the degeneracy between the thickness and the inclination angle of stellar disk, and a corresponding study of larger samples would be important for detection of evolutionary effects in disk properties.

ACKNOWLEDGMENTS. This study is based on observations made with the NASA/ESA Hubble Space Telescope, obtained from the data archive at the Space Telescope Science Institute. Our work was supported by the Estonian Science Foundation grants 7765, 8005, 9428, MJD272 and the projects SF0060067s08 and TK120 in (Astro)particle Physics and Cosmology (TK120). All the figures have been made using the Gnuplot plotting utility. We thank the TKRS group and B. Weiner for making their data publicly available and the anonymous referee for useful comments and suggestions.

REFERENCES

Chemin L., de Blok W. J. G., Mamon G. A. 2011, AJ, 142, 109
Conselice C. J. 2003, ApJS, 147, 1
Fathi K., Gatchell M., Hatziminaoglou E., Benoit E. 2012, MNRAS, 423, L112
Fernández Lorenzo M., Cepa J., Bongiovanni A. et al. 2010, A&A, 521, A27
Giavalisco M., Ferguson H. C., Koekemoer A. M. et al. 2004, ApJ, 600, L93
Jardel J. R., Gebhardt K., Shen J. et al. 2011, ApJ, 739, 21
Merritt D., Graham A. W., Moore B. et al. 2006, AJ, 132, 2685
Miller S.H., Bundy K., Sullivan M. et al. 2011, ApJ, 741, 115
Lackner C. N., Gunn J. E. 2012, MNRAS, 421, 2277
Mutchler M., Cox C. 2001, Instrument Science Report, ACS 2001-07
Navarro J. F., Ludlow A., Springel V. et al. 2010, MNRAS, 402, 21
Simard L., Mendel J. T., Patton D. R. et al. 2011, ApJS, 196, 11
Sirianni M., Jee M. J., Benítez N. et al. 2005, PASP, 117, 1049
Tamm A., Tenjes P. 2003, A&A, 403, 529
Tamm A., Tenjes P. 2005, A&A, 433, 31
Tamm A., Tenjes P. 2006, A&A, 449, 67
Tempel E., Tenjes P. 2006, MNRAS, 371, 1269
Tempel E., Tamm A., Tenjes P. 2010, A&A, 509, A91
Tempel E., Tuvikene T., Tamm A. et al. 2011, A&A, 526, A155
Tenjes P., Haud U., Einasto J. 1994, A&A, 286, 753
Tenjes P., Haud U., Einasto J. 1998, A&A, 335, 449
Weiner B. J. Willmer C. N. A., Faber S. M. et al. 2006, ApJ, 653, 1027
Wirth G. D., Willmer C. N. A., Amico P. et al. 2004, AJ, 127, 3121
York D. G., Adelman J., Anderson Jr. J. E. et al. 2000, AJ, 120, 1579